

© 2023 IEEE. Personal use of this material is permitted. Permission from IEEE must be obtained for all other uses, in any current or future media, including reprinting/republishing this material for advertising or promotional purposes, creating new collective works, for resale or redistribution to servers or lists, or reuse of any copyrighted component of this work in other works.

A Balanced Filtering Antenna Array With High Gain, Steep Selectivity, and Multi-Radiation Nulls Parallel-Fed by Differential Broadband Network

Feng Wei, Xinxin Liu, Xue-Zhi Ding, Xi-Bei Zhao, and Pei-Yuan Qin

Abstract—In this communication, a 2×2 balanced filtering antenna array parallel-fed by a differential broadband network is presented. The array has four identical stacked filtering antenna elements, each of which consists of a main patch etched with a folded U-shaped slot, a pair of ear-shaped parasitic patches, a stacked patch, and a folded T-shaped strip. The conceived antenna topology can enhance the gain flatness, improve selectivity, and increase the number of radiation nulls. Meanwhile, by introducing a novel ring-shaped transition structure (RSTS) to the balanced-to-single-ended (BTSE) four-way feeding network, a broad bandwidth, low insertion losses, low phase difference errors, and high common-mode (CM) suppression are realized. To validate the method, an integrated antenna array with a center frequency at 2.5 GHz is fabricated and measured. Experimental results exhibit a boresight gain of 13.7 dBi, four radiation nulls, and a square factor (SF_{10}) of 1.21.

Index Terms—Antenna array, balanced antenna, CM suppression, differential broadband network, filtering antenna, high gain, multi-radiation nulls, steep selectivity.

I. INTRODUCTION

With the increasing demand for wireless communication systems, antennas and filters have become essential in various applications. To address the need for more compact and efficient systems, integrating a bandpass filter and antenna into a single module known as a filtering antenna has gained significant attention [1], [2], [3], [4], [5]. This approach offers numerous benefits, including reduced volume, decreased insertion losses, and more efficient spectrum utilization. Over the past few decades, several studies on filtering antennas have been proposed. In the early days, the most common approach was to cascade filters and antennas directly, with the antennas serving as the last-stage resonator of the filter [6], [7]. While these filtering antennas exhibited good selectivity, the use of multiple resonators resulted in a large overall volume and high insertion losses. Then, an improved method emerged by modifying the feeding structures of antennas to achieve the desired filtering characteristics. For example, resonance structures were introduced to the feeding microstrip lines in [8], [9], [10], and the coupling apertures were adjusted in [11], [12], [13]. Furthermore, some structures such as U-shaped slots and stacked patches are employed to achieve filtering performances [14], [15]. These works eliminated the need for additional circuits, but the insertion losses remained high. It should be noted that most of the reported filtering antennas and arrays are single-end fed.

Balanced circuits offer significant advantages over single-ended circuits by providing immunity to the electromagnetic interference and environmental noise [16]. Researchers have focused on developing balanced-to-single-ended (BTSE) feeding networks for flexible connections between balanced circuits and single-ended antennas. Various studies have been proposed for BTSE feeding

networks using microstrip lines and slotlines [17], [18]. The microstrip-slotline transition (MST) offers natural common-mode (CM) suppression due to its physical structure [19]. However, the balanced ports required for CM suppression occupy considerable space [20]. Furthermore, multi-stage MSTs / slotline-microstrip transitions (SMTs) lead to extra insertion losses, narrower bandwidths, and high phase difference errors [21]. Additionally, it is challenging to achieve optimal integration between the BTSE feeding network and antenna elements. A properly designed BTSE network integrated into an array can effectively improve its functionality.

Due to the significant challenges to design high performance BTSE feeding network, it is found that very few works have been reported on balanced filtering antenna array. In [22], by side-feeding four patches applying a BTSE network, a 2×2 filtering antenna array is achieved. Although a simple structure and low cross-polarization levels are realized, its filtering performance and CM rejection can be improved further. In [23], by connecting a quasi-Yagi antenna and a bandpass filter directly, a filtering antenna is achieved. But it has low integration suitability, high insertion losses, and large volume. Hence, there is still a technology gap to design and implementation of a balanced filtering antenna array.

This communication presents a 2×2 balanced filtering antenna array parallel-fed by a differential broadband network. To the best of the authors' knowledge, only few works on differential filtering antenna array have been published. The proposed array consists of new filtering antenna elements including a folded T-shaped strip, a pair of ear-shaped parasitic patches and a planar BTSE broadband feeding network based on novel ring-shaped transition structure (RSTS). Different from the reported works using multi-stage MSTs/SMTs, there is only one-stage MST/SMT in the proposed network. Therefore, broad bandwidth, low insertion losses, low phase difference errors, high CM suppression, and ease of integration with single-ended antenna elements are realized. Additionally, by utilizing a broadband feeding network, it is easy to achieve a flat passband gain. Owing to the characteristics of the feeding network, the proposed filtering antenna array has the same advantages as the elements while increasing anti-interference abilities and higher gain. Overall, the proposed array offers new opportunities for improving system performance in wireless communication applications.

II. FILTERING PATCH ANTENNA ELEMENT

A. Antenna Configuration

In Fig. 1, the proposed element is composed of three-layer substrates which all are F4BM with a permittivity of 2.2 and a thickness of 0.8 mm. There are two air gaps h_1 and h_2 between the three-layer substrates. *Lyr. 1* is printed on the top layer of *Sub. 1*. *Lyr. 2* and *Lyr. 3* are printed on the top and bottom layers of *Sub. 2*, respectively. And *GND* is printed on the bottom layer of *Sub. 3*. The element is assembled firmly and precisely with nylon screws and gaskets. Fig. 2 (a) shows *Lyr. 1*, which consists of a stacked patch etched with a U-shaped slot. Fig. 2 (b) shows *Lyr. 2* which contains a

Manuscript received June 1, 2023; revised August 9, 2023; accepted August 28, 2023.

Feng Wei, Xinxin Liu, Xue-Zhi Ding, and Xi-Bei Zhao are with National Key Laboratory of Antennas and Microwave Technology and Xi'an Key Laboratory of Millimeter Wave and Terahertz Technologies, School of Electronic Engineering, Xidian University, Xi'an 710071, China (e-mail: fwei@mail.xidian.edu.cn).

Pei-Yuan Qin is with Global Big Data Technologies Centre, Faculty of Engineering and Information Technology, University of Technology Sydney, Sydney, Australia (email: Peiyuan.Qin@uts.edu.au).

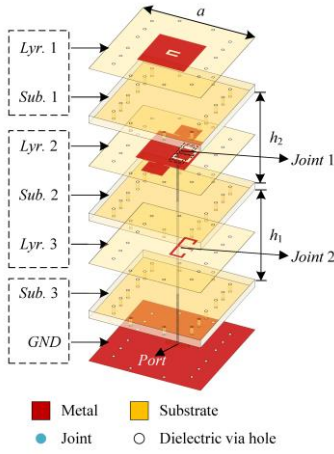


Fig. 1. Configuration of the proposed stacked filtering antenna element. ($a = 100$, $h_1 = 1.3$, $h_2 = 1$, unit: mm.)

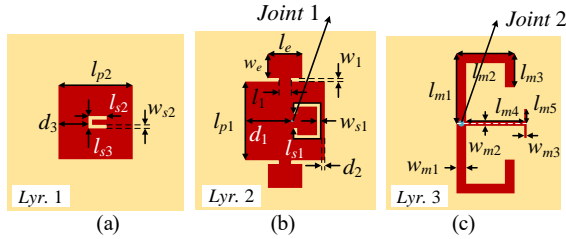


Fig. 2. Layout of (a) Lyr. 1, (b) Lyr. 2, and (c) Lyr. 3. ($d_1 = 26$, $d_2 = 2.3$, $d_3 = 17$, $l_{p1} = 44$, $l_{p2} = 42$, $l_e = 19$, $w_e = 15$, $l_1 = 6$, $w_1 = 0.5$, $l_{s1} = 62$, $l_{s2} = 10.3$, $l_{s3} = 7$, $w_{s1} = 2$, $w_{s2} = 2$, $l_{m1} = 14.5$, $l_{m2} = 12$, $l_{m3} = 7$, $l_{m4} = 12$, $l_{m5} = 3$, $w_{m1} = 2$, $w_{m2} = 1$, and $w_{m3} = 0.5$, unit: mm.)

main patch with a pair of ear-shaped parasitic patches and a folded U-shaped slot which is opposite to the slot on Lyr. 1. Fig. 2 (c) shows Lyr. 3 where printed a folded T-shaped strip. Notably, the proposed element is fed by a 50Ω SMA connector at the bottom layer of Sub. 3, which has three solder joints. As indicated by the dotted line in Fig. 1, the inner conductor of the SMA connector with a length of 2.9 mm passes through Sub. 2 and Sub. 3, and is soldered to the main patch and folded T-shaped strip at Joint 1 and Joint 2, respectively. The outer conductor of the connector is soldered to GND at the Port position.

B Working Mechanism

Fig. 3 shows the simulated S -parameters and boresight gain of the proposed element. As can be observed, the S -parameters exhibit three resonance frequencies (f_{r1} , f_{r2} , and f_{r3}) which constitute the passband. In addition, the boresight gain shows steep selectivity by introducing four radiation nulls (f_{n1} , f_{n2} , f_{n3} , and f_{n4}) distributed over the stopband. It should be mentioned that all the radiation nulls can be independently controlled. However, owing to the length limit, not all the analyses about the control are given. To explain the working mechanism of the element, analyses based on surface current distributions and characteristic mode analysis (CMA) are conducted.

Fig. 4 (a) and (b) depict the surface current distributions on Lyr. 2 at f_{r1} and f_{n2} , respectively. The results indicate that the currents are predominantly confined around the U-shaped slot etched on the main patch, forming a half-wavelength resonant structure at f_{r1} . The overall currents exhibit an in-phase distribution along the x -direction (co-polarization) at f_{r1} , while exhibiting an out-of-phase distribution along the y -direction (cross-polarization) at f_{n2} . Thus, the introduction of a resonance frequency f_{r1} and a radiation null f_{n2} can be attributed to the U-shaped slot etched on Lyr. 2. It should be

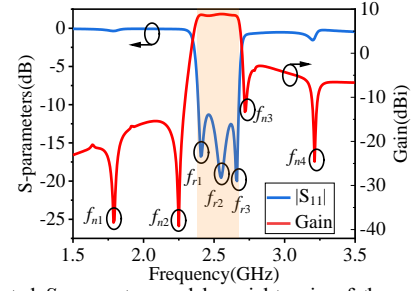


Fig. 3. Simulated S -parameters and boresight gain of the proposed stacked filtering patch antenna element.

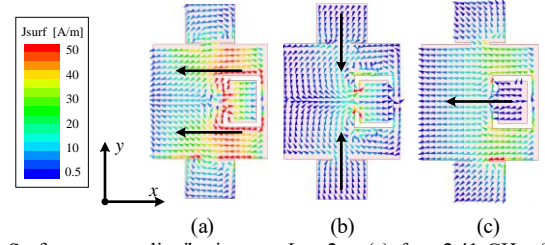


Fig. 4. Surface current distributions on Lyr. 2 at (a) $f_{r1} = 2.41$ GHz, (b) $f_{n2} = 2.25$ GHz, and (c) $f_{r2} = 2.55$ GHz.

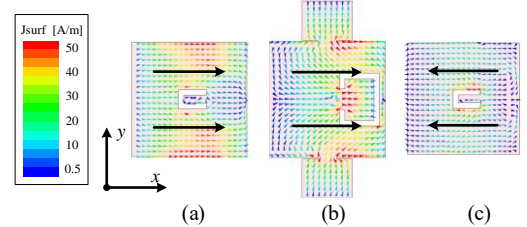


Fig. 5. Surface current distributions (a) on Lyr. 1 at $f_{r3} = 2.66$ GHz and on (b) Lyr. 2 and (c) Lyr. 1 at $f_{n3} = 2.73$ GHz.

mentioned that the introduction of the pair of ear-shaped patches is to adjust the impedance matching of the proposed filtering element easily.

In Fig. 4 (c), the surface current distributions on Lyr. 2 are presented at f_{r2} . Notably, the currents on the main patch are almost exactly in phase along the x -direction, indicating that f_{r2} is introduced by the main patch itself. Moreover, it is worth mentioning that the length of the radiating edge of the main patch is approximately one-half guidance wavelength at f_{r2} .

Surface current distributions at f_{r3} and f_{n3} are depicted in Fig. 5 (a) and (b), respectively. At f_{r3} , the currents are primarily concentrated on the stacked patch on Lyr. 1, exhibiting an in-phase distribution along the x -direction. The length of the patch on Lyr. 1 is one-half guidance wavelength at f_{r3} . However, the currents on Lyr. 1 and Lyr. 2 flow in opposite directions at f_{n3} , resulting in the cancellation of currents on the two layers and a decrease in radiation efficiency. Notably, the small U-shaped slot etched on Lyr. 1 is utilized to adjust the coupling of the stacked patch and the main one.

To illustrate the mechanism of the folded T-shaped strip, characteristic mode analysis (CMA) utilizing the simulation software CST Microwave Studio (CST MWS) is adopted to investigate the operating principle. Considering that the folded T-shaped strip and the inner conductor of the SMA connector are soldered together at Joint 2, Joint 2 acts as a short-circuited point. The folded T-shaped strip on the top of a grounded dielectric layer with a height of 0.8 mm is shown in Fig. 6 (a), and the corresponding modal significances (MSs) of the characteristic modes are shown in Fig. 6 (b). Modes 1 and 2 are generated at frequencies of 1.92 and 3.34 GHz, respectively. The corresponding modal current distributions at corresponding frequencies are shown in Fig. 7 (a) and (b), respectively, where the black arrows indicate the directions of the

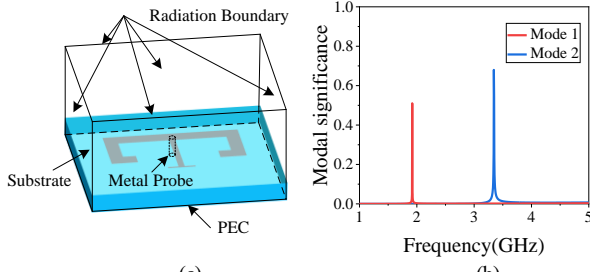


Fig. 6. (a) Geometrical modeling and boundary setup. (b) MSS.

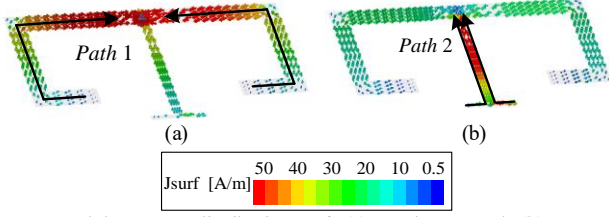


Fig. 7. Modal current distributions of (a) modes 1 and (b) 2 at the corresponding resonance frequencies.

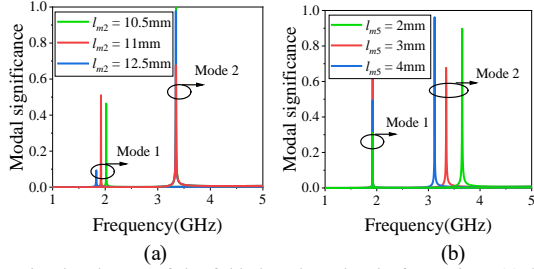


Fig. 8. Simulated MSSs of the folded T-shaped strip for various (a) l_{m2} and (b) l_{m5} .

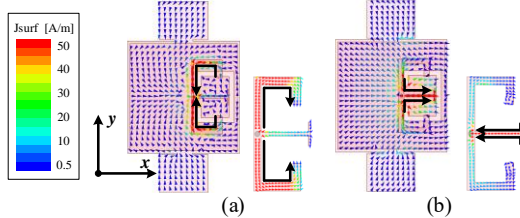


Fig. 9. Surface current distributions on *Lyr.* 2 and *Lyr.* 3 at (a) $f_{n1} = 1.79$ GHz and (b) $f_{n4} = 3.21$ GHz.

current. Furthermore, modes 1 and 2 of the folded T-shaped strip resonate along paths 1 and 2, respectively. Fig. 8 (a) and (b) demonstrate the effects of parameters l_{m2} and l_{m5} on the corresponding MSSs. It is important to note that only one parameter (l_{m2} or l_{m5}) is changed each time, while the other parameters remained unchanged. In Fig. 8 (a), as l_{m2} increases from 10.5 to 13.5 mm, the resonance frequencies of mode 2 remain unchanged, while the resonance frequencies of mode 1 shift to the lower frequencies. In Fig. 8 (b), as l_{m5} increases from 2 to 4 mm, the resonance frequencies of mode 1 remain unchanged, while the resonance frequencies of mode 2 shift to the lower frequencies. Therefore, the two resonance modes of the folded T-shaped strip are independently controllable.

Fig. 9 (a) and (b) give the surface current distributions on *Lyr.* 2 and *Lyr.* 3, respectively. As can be seen in Fig. 9 (a), the resonant mode of the folded T-shaped strip is identical to mode 1 utilizing CMA in Fig. 7 (a). The same is true for Fig. 9 (b) and Fig. 7 (b). In addition, when it resonates as shown in Fig. 9 (a) and (b), almost all energy is concentrated in the space where the strip is located. Moreover, the directions of the strong surface currents of the folded

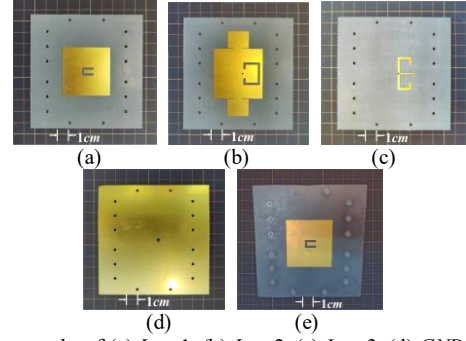


Fig. 10. Photographs of (a) *Lyr.* 1, (b) *Lyr.* 2, (c) *Lyr.* 3, (d) *GND*, and (e) the assembled antenna element.

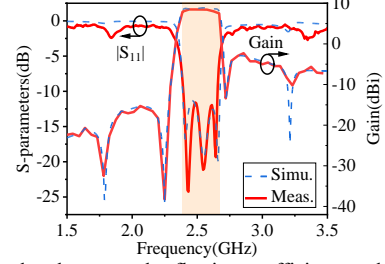


Fig. 11. Simulated and measured reflection coefficients and boresight gain of the proposed stacked filtering antenna element.

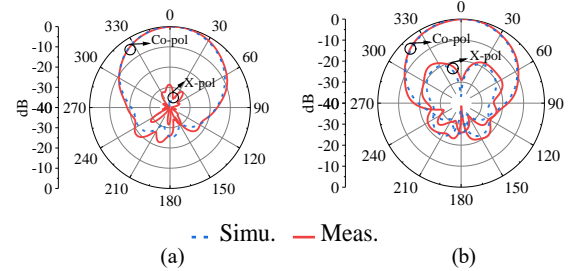


Fig. 12. Simulated and measured radiation patterns at the center frequency of 2.5 GHz in (a) xoz and (b) yoZ plane.

T-shaped strip and main patch are opposite, leading to the energy cancellation and the introduction of two independently controllable radiation nulls (f_{n1} and f_{n4}).

C. Measurement Verification

To verify the performance of the proposed element, the prototype was fabricated and measured as shown in Fig. 10. In this communication, the reflection coefficients of the prototype were measured using an Agilent VNA (vector network analyzer) N5230A. Additionally, the boresight gain and radiation patterns were obtained in an anechoic chamber.

Fig. 11 and Fig. 12 show the simulated and measured results of the proposed element. The measured (simulated) $|S_{11}|$ reveals three resonance frequencies at 2.43, 2.54, and 2.64 GHz (2.41, 2.55, and 2.66 GHz), respectively. The -10-dB impedance bandwidth is 10.8% (2.39 GHz - 2.66 GHz) for the measured datas and 11.6% (2.39 GHz - 2.68 GHz) for the simulated datas with a center frequency at 2.5 GHz. The measured (simulated) boresight gain is about 8.46 (8.89) dBi. To characterize the gain flatness of the proposed element, an indicator $\Delta G/BW_G$ is defined. BW_G is the fraction bandwidth (FBW) of the gain stable range, and ΔG is the maximum gain fluctuation. The proposed element accomplished a fairly flat gain response with a measured (simulated) $\Delta G/BW_G$ of 0.52 dB/9.5% (0.38 dB/10.4%). However, in the stopband of the antenna, four radiation nulls are presented, which yield stopband suppression levels of 10.74 (11.76)

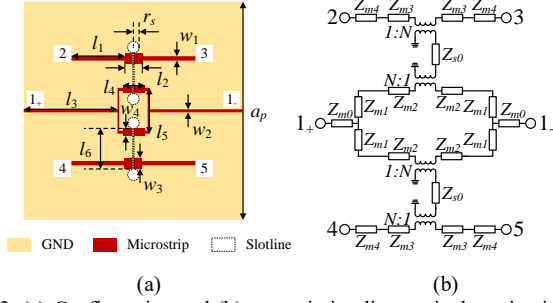


Fig. 13. (a) Configuration and (b) transmission-line equivalent circuit of the proposed BTSE feeding network. ($a_p = 200$, $l_1 = 52$, $l_2 = 9$, $l_3 = 85.5$, $l_4 = 12$, $l_5 = 36.43$, $l_6 = 38.5$, $w_1 = 2.43$, $w_2 = 2.43$, $w_3 = 6$, $w_4 = 5$, and $r_s = 3$, unit: mm. $Z_{m0} = 46$, $Z_{m1} = 65$, $Z_{m2} = 45$, $Z_{m3} = 50$, $Z_{m4} = 65$, and $Z_{s0} = 80$, unit: Ω .)

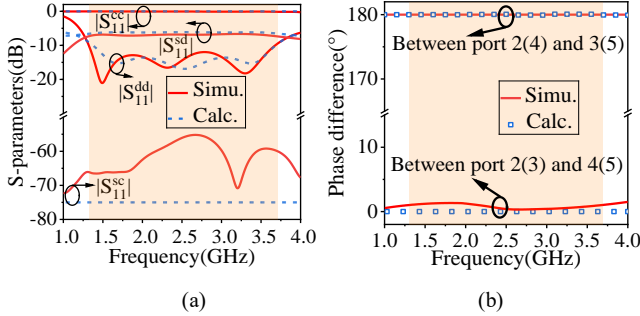


Fig. 14. Comparison between simulated and calculated (a) S-parameters and (b) phase difference of four output ports.

dB and 23.74 (24.28) dB at the higher and lower frequencies in measurement (simulation), respectively.

The selectivity of filtering antenna elements can be characterized by a concept similar to the square factor (SF) in filters. And the closer the SF is to 1, the better the selectivity of the filtering antenna:

$$SF_{10} = BW_{10}/BW_3 \quad (1)$$

BW_{10} and BW_3 are the bandwidth where the gain is reduced by 10 dB and 3 dB from the maximum boresight gain, respectively. Thus, the measured (simulated) SF_{10} of the proposed element is 1.14 (1.17), indicating the excellent selectivity.

The radiation patterns of the proposed antenna element were measured and simulated at the center frequency of 2.5 GHz in xoz and yoZ planes, as shown in Fig. 12 (a) and (b). The results demonstrate broadside radiation patterns with measured (simulated) 3-dB beam widths of approximately 66° (64°) in xoz plane and 71° (68°) in yoZ plane, respectively. Additionally, the measured (simulated) cross-polarization levels in the boresight direction in xoz and yoZ plane are -28.8 (-36.76) dB and -28.8 (-33.7) dB, respectively, indicating excellent rejection of cross-polarization.

The simulated results reasonably agree with the measured ones, except for some minor discrepancies that can be attributed to the fabrication tolerances and assembly accuracies. Overall, these findings suggest that the proposed element is an effective solution for achieving great filtering response with steep selectivity and multi-radiation nulls.

III. BALANCED STACKED FILTERING ANTENNA ARRAY

A. Balanced-to-Single-Ended Feeding Network

Fig. 13 (a) shows the configuration of the proposed BTSE feeding network, which is fabricated on an F4BM substrate, identical to the aforementioned element. The ground plane and microstrip lines are printed on the bottom and top layers of the substrate, respectively, while the slotlines are etched on the ground plane. The BTSE

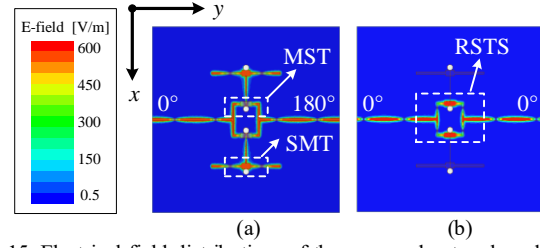


Fig. 15. Electrical field distributions of the proposed network under (a) DM and (b) CM excitations at 2.5 GHz.

feeding network comprises microstrip T-junctions, MSTs, SMTs, a pair of balanced input ports, and four single-ended output ports.

Fig. 13 (b) illustrates the transmission-line equivalent circuit of the proposed network, where Z_{mk} ($k = 0, 1, 2, 3, 4$) and Z_{sk} ($k = 0$) represent the characteristic impedances of microstrip lines and slotlines, respectively. To characterize the transition between the microstrip line and slotline, multiple $N:1$ transformers have been introduced. Ideally, the electrical lengths of all the transmission lines are set as 90° at the center frequency of 2.5 GHz, and N is set as 1. Furthermore, the values of the calculated impedances by simulation software Advanced Design System (ADS) are also given in Fig. 10.

In Fig. 14, comparisons between the calculated results obtained by ADS and the simulated ones obtained by HFSS are given. Owing to the network's symmetry and the article length constraint, only $|S_{21}^{sd}|$ and $|S_{21}^{sc}|$ are given, while $|S_{31}^{sd}|$, $|S_{41}^{sd}|$, $|S_{51}^{sd}|$, $|S_{31}^{sc}|$, $|S_{41}^{sc}|$, and $|S_{51}^{sc}|$ are omitted. The comparison shows a good agreement between the calculated and simulated results. Fig. 14 (a) illustrates the broadband differential-mode (DM) transmission and high CM suppression, with a -10 -dB impedance bandwidth covering 1.32 - 3.68 GHz (simulated) and 1.35 - 3.66 GHz (calculated). The corresponding FBW is 94.2% (simulated) and 92.4% (calculated).

The DM transmission coefficient $|S_{21}^{sd}|$ represents the energy division from differential port 1 to other single-ended ports. As observed in Fig. 14 (a), the energy is evenly divided, with insertion losses ranging from about 0.65 - 1.52 dB (simulated) and 0.15 - 1.18 dB (calculated) under DM excitations. Furthermore, the CM reflection coefficient $|S_{11}^{cc}|$ is nearly 0 dB over the entire operating bandwidth. It should be mentioned that the calculated S_{21}^{cc} is far below -75 dB. Considering the clarity and aesthetics of the figure, S_{21}^{cc} in Fig. 14 is set to -75 dB. The simulated S_{21}^{cc} is lower than -50 dB. Hence, great CM suppression is achieved. Fig. 14 (b) gives the phase relationships between four output ports under DM excitations. The simulated (calculated) phase differences between port 2 (4) and port 3 (5) are 180° , while those between port 2 (3) and 4 (5) are almost 0° over the entire frequency range. Hence, the proposed feeding network achieves broadband, high CM suppression, low insertion losses, and low phase errors.

To further demonstrate the effectiveness of the proposed network in achieving DM transmission and CM suppression, electrical field distributions under DM and CM excitations at 2.5 GHz are given in Fig. 15. As can be observed, only DM signals can be transmitted through the MST and distributed to the single-ended ports, while CM signals are canceled out at the MST, resulting in negligible CM energy transmission from input ports to output ones.

Fig. 16 depicts the schematic diagram of signal flow of the proposed feeding network. All CM signals cannot flow out of the RSTS. As they are transmitted to the MST, a virtual magnetic wall is created so that the CM signals cannot be converted to the slotline mode, resulting in great CM suppression [19]. Notably, the introduction of the RSTS eliminates the implementation of multi-stage MSTs (SMTs) commonly employed in conventional BTSE networks based on microstrip lines and slotlines. Thus, the proposed

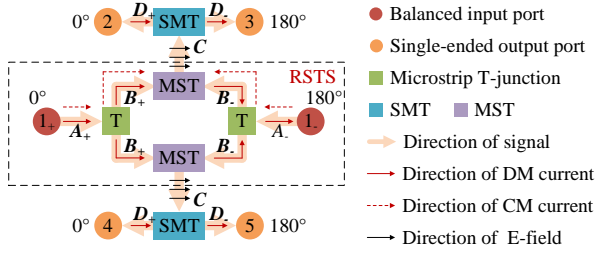


Fig. 16. Schematic diagram of signal flow of the proposed BTSE broadband network.

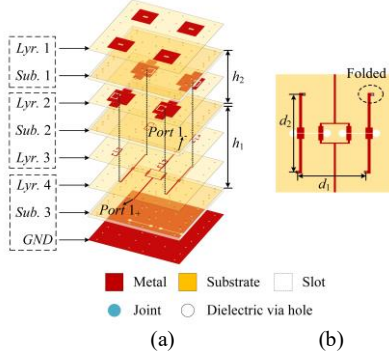


Fig. 17. Configuration of (a) the proposed differential-parallel-fed stacked filtering antenna array and (b) Lyr. 4. ($d_1 = 100$ and $d_2 = 111$, unit: mm.)

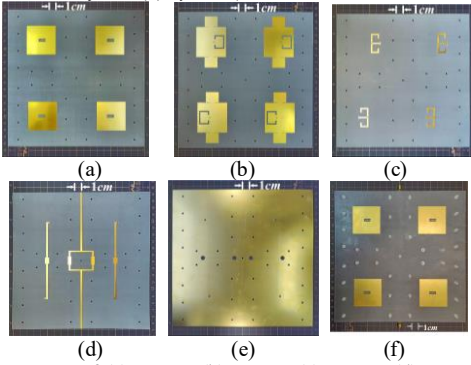


Fig. 18. Prototypes of (a) Lyr. 1, (b) Lyr. 2, (c) Lyr. 3, (d) Lyr. 4, (e) GND, and (f) the assembled differential-parallel-fed stacked filtering antenna array.

BTSE feeding network exhibits excellent CM suppression, broadband transmission characteristics, and low phase difference errors.

B Stacked Filtering Antenna Array Parallel-Fed by Differential Broadband Network

The proposed differential broadband network and four antenna elements designed in Section II are combined to achieve a 2×2 parallel-fed balanced filtering antenna array, as shown in Fig. 17 (a). Considering the phase differences of the outputs of the network, antenna elements are placed in opposite pairs as shown in Fig. 17 (a). To optimize the arrangement of the elements, the microstrip lines at the four outputs of the feeding network are folded as shown in Fig. 17 (b). And four metal probes are applied to connect the network and the elements. To verify its performance, the prototype is fabricated and measured. The photographs of the proposed filtering array are depicted in Fig. 18.

It should be mentioned that a 180° coupler which can provide DM and CM signals is utilized in the gain measurement. The comparisons between the measured and simulated reflection coefficients and boresight gain are illustrated in Fig. 19. The -10 -dB impedance bandwidth is 12% (2.41 GHz - 2.71 GHz) for the

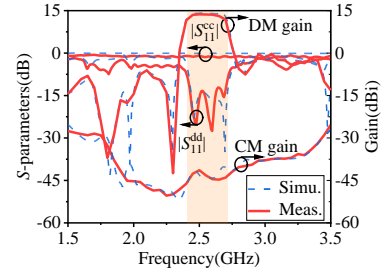


Fig. 19. Simulated and measured reflection coefficients and boresight gain of the proposed differential-parallel-fed stacked filtering antenna array.

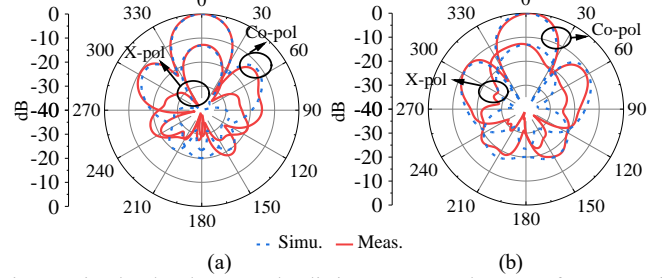


Fig. 20. Simulated and measured radiation patterns at the center frequency of 2.5 GHz in (a) xoz plane and (b) yoZ plane.

measured datas and 12% (2.42 GHz - 2.72 GHz) for the simulated datas with a center frequency at 2.5 GHz. Furthermore, the CM reflection coefficients are higher than -1.95 (-0.12) dB over the whole bandwidth in measurement (simulation). And the measured and simulated CM gains are all lower than -26.2 dBi, exhibiting a great CM suppression. The maximum measured (simulated) boresight gain is 13.7 (14.2) dBi across the entire operating bandwidth, demonstrating a gain improvement of 5.24 dB compared to the single element. The proposed filtering antenna element accomplished a fairly flat gain response with a measured (simulated) $\Delta G/BW_G$ of 0.62 dB/8% (0.6 dB/10.4%). Additionally, the multiple radiation nulls yield measured (simulated) stopband suppression levels of 13.92 (13.27) dB and 19.74 (22.47) dB at the higher and lower frequencies, respectively. Importantly, the measured (simulated) SF_{10} of the proposed array is 1.21 (1.21), indicating excellent selectivity. Therefore, the efficient radiation and bandpass filtering responses are implemented in the 2×2 array.

In Fig. 20 (a) and (b), the measured and simulated radiation patterns at the center frequency of 2.5 GHz in xoz and yoZ planes of the proposed array are given. Notably, the beam exhibits a bunched pattern due to the implementation of the 2×2 array compared to the single element. The measured (simulated) 3-dB beam width is about 30° (30°) in both xoz and yoZ planes. Additionally, in the boresight direction, the measured (simulated) cross-polarization levels are -12.83 (-13.13) dB in xoz plane and -13.13 (-13.13) dB in yoZ plane, respectively. The cross polarization can be attributed to the radiation leakage of the slotlines in the proposed feeding network.

As can be observed, good consistency between the simulation and measurement is achieved. Table I lists a comprehensive comparison between the proposed array and several reported corresponding works. As can be observed, comparing with differential filtering arrays [21], [22], the proposed design features better performance in terms of the gain, selectivity, CM suppression, flat gain response, and multiple radiation nulls.

IV. CONCLUSION

In this communication, a balanced filtering antenna array differential-parallel-fed by a broadband feeding network is

TABLE I
COMPARISON BETWEEN THE PROPOSED DESIGN AND REPORTED WORKS

Design	[5]	[10]	[13]	[21]	[22]	This work
Element number	2×2	2×2	2×2	1×4	2×2	2×2
Size (λ_c^2)	1.18×1.13	1.74×1.74	1.45×2.22	5.77×1.87	1.20×1.20	2.14×1.66
Layer	1	2	2	1	2	3
Center frequency (GHz)	5	5.2	3	6.9	3.55	2.5
FBW(%)	3	10	37.1	74.7	6.5	12
Filtering response	Yes	Yes	Yes	No	Yes	Yes
Gain (dBi)	≤9.6	≤10.5	≤12.4	≤12.24	≤8.3	≤ 13.7
Radiation null	2	1	3	/	1	4
differential input	No	No	No	Yes	Yes	Yes
CM gain (dBi)	/	/	/	-13.8	-15	-26.2
Suppression levels of higher/lower frequencies(dB)	25.56/23.1	16.44/15.99	20.88/27.03	/	18.93/17.16	13.92/19.74
AG/BW_G^{**} (dB/%)	0.65/1	0.68/4	0.97/22	/	0.7/3	0.62/8
SF_{10}^{***}	1.53	1.37	1.14	/	1.53	1.21

* $SF_{10} = BW_{10}/BW_3$, BW_{10} (BW_3) is the bandwidth where the gain is reduced by 10 (3) dB from the maximum boresight gain.

** AG/BW_G , BW_G is the FBW of the gain stable range, and AG is the maximum gain fluctuation.

*** Some indicators were not given in the reported works, so we made rough estimates based on the provided data.

presented. The configurations and working mechanisms of the filtering antenna element, feeding network, and 2×2 array have been described in details. The filtering antenna element shows a great selectivity and a high gain. The differential broadband feeding network shows high CM suppression, low insertion losses, wide bandwidth, low phase difference errors, and great integration suitability with the antenna element due to the introduction of RSTS. As a result, the proposed balanced filtering array demonstrates very good anti-interference abilities. Furthermore, the simulated results and measured ones are in good agreement. In conclusion, due to the merits of high gains, steep selectivity, multi-radiation nulls, high integration, and strong anti-interference ability, the developed array is useful for balanced narrowband RF front-end chains for RFID, WiMAX, and radar systems.

REFERENCES

- [1] S. F. Wu, J. X. Li, X. M. Chen, S. Yan, and X. Y. Zhang, "A Ka-Band SLM Printed Filtering Divider-Fed Magnetolectric Dipole Antenna Array Using Embedded Gap Waveguide," *IEEE Antennas Wireless Propag. Lett.*, vol. 22, no. 4, pp. 774-778, Apr. 2023.
- [2] H. F. Su, L. L. Wu, Y. Zhang, H. L. Xu, and X. Y. Zhang, "Analysis and Design of Filtering Series-Feed Omni-Directional Antenna for V2X Application," *IEEE Trans. Antennas Propag.*, vol. 70, no. 12, pp. 11485-11495, Dec. 2022.
- [3] J. -F. Qian, S. Gao, H. Y. Wang, H. Zhou, H. L. Xu, and L. H. Wen, "A Filtering Antenna Using Transversal Coupling Topology," *IEEE Antennas Wireless Propag. Lett.*, vol. 21, no. 12, pp. 2342-2346, Dec. 2022.
- [4] X. K. Liu, S. Gao, W. Hu, L. H. Wen, Q. Luo, B. Sanz-lzquierdo, X. D. Chen, L. Qian, J. T. Sumantyo, and X. -X. Yang, "A Compact Dual-Polarized Filtering Antenna With Steep Cut-Off for Base-Station Applications," *IEEE Trans. Antennas Propag.*, vol. 70, no. 7, pp. 5941-5946, Jul. 2022.
- [5] C.-K. Lin and S.-J. Chung, "A filtering microstrip antenna array," *IEEE Trans. Microw. Theory Techn.*, vol. 59, no. 11, pp. 2856-2863, Nov. 2011.
- [6] W. J. Wu, Y.-Z. Yin, S. L. Zuo, Z.-Y. Zhang, and J.-J. Xie, "A new compact filter-antenna for modern wireless communication systems," *IEEE Antennas Wireless Propag. Lett.*, vol. 10, pp. 1131-1134, 2011.
- [7] C.-T. Chuang and S.-J. Chung, "Synthesis and design of a new printed filtering antenna," *IEEE Trans. Antennas Propag.*, vol. 59, no. 3, pp. 1036-1042, Mar. 2011.
- [8] P. F. Hu, Y. M. Pan, X. Y. Zhang, and B.-J. Hu, "A filtering patch antenna with reconfigurable frequency and bandwidth using F-shaped probe," *IEEE Trans. Antennas Propag.*, vol. 67, no. 1, pp. 121-130, Jan. 2019.
- [9] J.-F. Qian, F.-C. Chen, Y.-H. Ding, H.-T. Hu, and Q.-X. Chu, "A wide stopband filtering patch antenna and its application in MIMO system," *IEEE Trans. Antennas Propag.*, vol. 67, no. 1, pp. 654-658, Jan. 2019.
- [10] C.-X. Mao, S. Gao, Y. Wang Y, F. Qin, and Q.-X. Chu, "Multimode resonator-fed dual-polarized antenna array with enhanced bandwidth and selectivity," *IEEE Trans. Antennas Propag.*, vol. 63, no. 12, pp. 5492-5499, Dec. 2015.
- [11] C.-Y. Hsieh, C.-H. Wu, and T.-G. Ma, "A compact dual-band filtering patch antenna using step impedance resonators," *IEEE Antennas Wireless Propag. Lett.*, vol. 14, pp. 1056-1059, 2015.
- [12] Y. M. Pan, P. F. Hu, X. Y. Zhang, and S. Y. Zhang, "A low-profile high-gain and wideband filtering antenna with metasurface," *IEEE Trans. Antennas Propag.*, vol. 64, no. 5, pp. 2010-2016, May. 2016.
- [13] Y.-M. Zhang, S. Zhang, G. W. Yang, and G. F. Pedersen, "A wideband filtering antenna array with harmonic suppression," *IEEE Trans. Microw. Theory Techn.*, vol. 58, no. 10, pp. 4327-4339, Oct. 2020.
- [14] X. Y. Zhang, W. Duan, and Y. -M. Pan, "High-Gain Filtering Patch Antenna Without Extra Circuit," *IEEE Trans. Antennas Propag.*, vol. 63, no. 12, pp. 5883-5888, Dec. 2015.
- [15] J. Y. Yin, T. L. Bai, J. Y. Deng, J. Ren, D. Q. Sun, Y. Zhang, and L. X. Guo, "Wideband single-layer substrate integrated waveguide filtering antenna with U-shaped slots," *IEEE Antennas Wireless Propag. Lett.*, vol. 20, no. 9, pp. 1726-1730, Sep. 2021.
- [16] J.-X. Chen, J. Li, and J. Shi, "Miniaturized dual-band differential filter using dual-mode dielectric resonator," *IEEE Microw. Wireless Compon. Lett.*, vol. 28, no. 8, pp. 657-659, Aug. 2018.
- [17] H. Zhu, J.-Y. Lin, and Y. J. Guo, "Filtering balanced-to-single-ended power dividers with wide range and high level of common-mode suppression," *IEEE Trans. Microw. Theory Techn.*, vol. 67, no. 12, pp. 5038-5048, Dec. 2019.
- [18] L. Li, W. Cheng, L.-S. Wu, J.-F. Mao, M. Tang, and X.-W. Gu, "A wideband filtering balanced-to-unbalanced out-of-phase power divider," *IEEE Microw. Wireless Compon. Lett.*, vol. 28, no. 10, pp. 870-872, Oct. 2018.
- [19] F. Wei, X.-B. Zhao, L. Xu, C. Zeng, and X. W. Shi, "Single-ended-to-balanced broadband/filtering planar magic-Ts with high common-mode suppression," *IEEE Trans. Microw. Theory Techn.*, vol. 69, no. 7, pp. 3236-3245, Jul. 2021.
- [20] J. Shi, K. Xu, W. Zhang, J.-X. Chen, and G. H. Zhai, "An approach to 1-to-2ⁿ way microstrip balanced power divider," *IEEE Trans. Microw. Theory Techn.*, vol. 64, no. 12, pp. 4222-4231, Dec. 2016.
- [21] F. Wei, J. X. Wang, X.-B. Zhao, C. Zeng, and J. Q. Hou, "Balanced-to-single-ended four-way out-of-phase power divider and its application to broadband balanced Quasi-Yagi antenna array," *IEEE Antennas Wireless Propag. Lett.*, vol. 19, no. 8, pp. 1370-1374, Aug. 2020.
- [22] H.-T. Hu, F.-C. Chen, J.-F. Qian, and Q.-X. Chu, "A differential filtering microstrip antenna array with intrinsic common-mode rejection," *IEEE Trans. Antennas Propag.*, vol. 65, no. 12, pp. 7361-7365, Dec. 2017.
- [23] F. Wei, X. -B. Zhao, and X. W. Shi, "A Balanced Filtering Quasi-Yagi Antenna With Low Cross-Polarization Levels and High Common-Mode Suppression," *IEEE Access*, vol. 7, pp. 100113-100119, Jul. 2019.